Axel Loewe*, Yan Xu, Eberhard P. Scholz, Olaf Dössel, and Gunnar Seemann

Understanding the cellular mode of action of vernakalant using a computational model: answers and new questions

Abstract: Vernakalant is a new antiarrhythmic agent for the treatment of atrial fibrillation. While it has proven to be effective in a large share of patients in clinical studies, its underlying mode of action is not fully understood. In this work, we aim to link experimental data from the subcellular, tissue, and system level using an in-silico approach. A Hill's equation-based drug model was extended to cover the frequency dependence of sodium channel block. Two model variants were investigated: M1 based on subcellular data and M2 based on tissue level data. 6 action potential (AP) markers were evaluated regarding their dose, frequency and substrate dependence. M1 comprising potassium, sodium, and calcium channel block reproduced the reported prolongation of the refractory period. M2 not including the effects on potassium channels reproduced reported AP morphology changes on the other hand. The experimentally observed increase of ERP accompanied by a shortening of APD_{90} was not reproduced. Thus, explanations for the drug-induced changes are provided while none of the models can explain the effects in their entirety. These results foster the understanding of vernakalant's cellular mode of action and point out relevant gaps in our current knowledge to be addressed in future in-silico and experimental research on this aspiring antiarrhythmic agent.

Keywords: antiarrythmic drug; atrial fibrillation; mathematical model; mode of action; vernakalant

DOI: 10.1515/CDBME-2015-0101

1 Introduction

Atrial fibrillation (AF) is the most common sustained arrhythmia in humans affecting almost 2% of the population in the developed world [1]. As the two major strategies ablation therapy and drug therapy fail to succeed in about one third of all patients, AF is still a major challenge motivating the search for new drugs. Current antiarrhythmic agents suffer from limited efficacy or severe side-effects such as provoking life-threatening torsades de pointes arrhythmia in the ventricles. Vernakalant is a new multichannel blocker for pharmacological cardioversion of AF and proved to be superior to both placebo and the existing intravenous agent amiodarone in several clinical studies [1]. Despite its clinical efficacy, the underlying mode of action on atrial myocytes is not understood. One experimental study investigated the effect on isolated ion channels [2]. Wettwer et al. assessed the effect on tissue preparations [3] and Dorian et al. [4] studied the effect on atrial and ventricular refractory period in humans. However, these results on different integration levels could not be linked until now. In this work, we try to elucidate the complex non-linear effects of vernakalant on the cellular level by linking the experimental data from the single channel level to tissue level data.

***Corresponding Author: Axel Loewe:** Institute of Biomedical Engineering, Karlsruhe Institute of Technology (KIT), Kaiserstr. 12, 76128 Karlsruhe, E-mail: publications@ibt.kit.edu

Yan Xu, Olaf Dössel, Gunnar Seemann: , Institute of Biomedical Engineering, Karlsruhe Institute of Technology (KIT), Karlsruhe, Germany

Eberhard P. Scholz: Department of Internal Medicine III, University Hospital Heidelberg, Heidelberg, Germany

2 Methods

2.1 Electrophysiological model

Cellular electrophysiology was modeled using the Courtemanche-Ramirez-Nattel model of human atrial myocytes [5] in the *Control* case. To represent chronic AF (*cAF*) induced remodeling, several conductivities were altered as described before [6]. In brief, I_{to} was reduced by 65%, I_{K1} was increased by 100%, I_{Ks} was increased by 100%, I_{Kur} was reduced by 50%, I_{CaL} was reduced by 55%, $I_{Na,Ca}$ was increased by 60%, and the SR leak current was increased by 50%. Furthermore, the cell capacitance was increased by 20%.

An implementation of the monodomain model [7] was utilized to simulate excitation propagation in a one-dimensional tissue strand of size $20 \times 0.1 \times 0.1\,mm^3$. The domain was discretized by cubic voxels with a side length of $0.1\,mm$. The monodomain conductivity was set to

Table 1: Frequency-dependent IC_{50} / nH estimations for I_{Na} based on dV_m/dt_{max} reduction data [3].

		M1		M2	
		IC_{50} (μM)	nH	IC_{50} (μM)	nH
Control	**0.5 Hz**	36.15	2.67	35.79	2.67
	1.0 Hz	36.25	1.16	35.27	1.07
	3.0 Hz	15.07	0.95	17.34	1.25
cAF	**0.5 Hz**	76.89	1.26	39.45	1.87
	1.0 Hz	61.32	1.10	61.88	1.18
	3.0 Hz	36.99	1.27	37.32	1.10

76 mS/m yielding a conduction velocity of 750 mm/s in the *Control* model without any drug-induced changes at a frequency of 1 Hz. Each voxel of the system was initialized in a single-cell environment for 50 beats followed by 5 beats in the tissue strand to adapt to the stimulation frequency. Stimuli were applied in voxels # 0..2, action potentials (APs) were evaluated in voxel # 150 as described before [8].

2.2 Drug model

Vernakalant reduces the conductance of several atrial ionic currents. We modeled its effect based on Hill's equation:

$$\Theta = \frac{1}{1 + \left(\frac{IC_{50}}{D}\right)^{nH}} \quad (1)$$

with Θ being the degree of channel blockage ranging from 0 to 1, IC_{50} being the half maximal inhibitory concentration, D being the free drug concentration, and nH being the Hill coefficient. The IC_{50} / nH values for the different currents were extracted from literature for model 1 (M1): 21.0 μM / 0.92 for I_{Kr} [2], 13.0 μM / 0.92 for I_{Kur} [2], 30.0 μM / 0.82 for I_{to} [2], and 84.0 μM / 1.0 for I_{CaL} [3]. As a hypothesis, a second model M2 was defined with only I_{CaL} being affected (42.0 μM / 1.0) besides the sodium channel block considered in both M1 and M2.

Due to the frequency dependence of I_{Na} block, it can not be represented by a single IC_{50}/nH value pair. Instead, we chose to determine the degree of I_{Na} block (g_{Na} reduction) by matching experimentally found reduction of the upstroke velocity dV_m/dt_{max} for each frequency and vernakalant concentration individually. Towards this end, dV_m/dt_{max} at zero drug concentration was taken as a reference value and the I_{Na} block in the drug model was tuned to match the experimentally found relative reduction in dV_m/dt_{max} [3]. This optimization was performed in the tissue strand environment described above. Using the degrees of block at 10 μM and 30 μM, frequency-specific IC_{50} / nH value pairs were estimated.

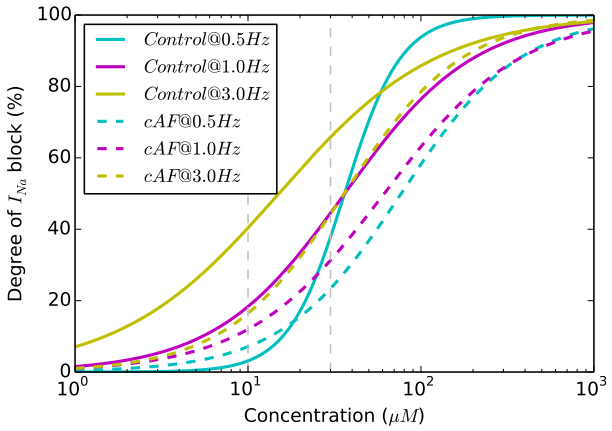

Figure 1: Frequency- and substrate-dependent degree of I_{Na} block based on the values for M1 in Table 1. The vertical lines indicate the concentration range investigated in the study by Wettwer et al. [3].

3 Results

The bisection-based tuning of g_{Na} reduction aiming at a replication of experimentally observed dV_m/dt_{max} reduction converged for all substrates, frequencies, and concentrations. The resulting degree of g_{Na} block is shown in Table 2. The degree of I_{Na} block increased with increasing frequency as can be seen from the frequency-specific IC_{50} and nH values in Table 1. This effect is reflected in lower IC_{50} values as well as in reduced Hill coefficients. Figure 1 reveals that this resulted in a consistently higher degree of block for higher frequencies within a concentration range of 1 – 35 μM. The frequency dependence was less pronounced in the *cAF* substrate than in *Control*.

The in-silico drug models were used to simulate a train of APs in the tissue strand environment (see Figure 2). In the *Control* substrate, 2:1 block occured at 3 Hz stimulation frequency using the drug model M1. For all other combinations, APs could be induced continuously, although alternans was observed in some of the models. Besides the upstroke velocity, 6 further AP markers were evaluated for the 6^{th} AP: effective refractory phase (ERP), AP duration at 90% and 20% repolarization (APD_{90}, APD_{20}), AP amplitude (APA), resting membrane potential (RMP), and PLT_{20} defined as the mean potential in the time window between 20% and 30% repolarization. Table 2 shows the results in comparison to the experimentally observed values in [3]. Model M1 reproduced the ERP prolongation seen in [3].

Table 2: Resulting g_{Na} reduction based on dV_m/dt_{max} tuning and AP markers obtained using the two in-silico models M1 and M2 in comparison to experimentally observed data [3].

				g_{Na}	dV_m/dt_{max}	ERP	APD_{90}	APD_{20}	PLT_{20}	APA	RMP
Control	0.5 Hz	10 μM	M1	-3.1%	-8.3%	+4.1%	+3.8%	+31.0%	-0.0%	-1.4%	-0.2%
			M2	-3.1%	-6.4%	-0.6%	-0.7%	-86.1%	+8.4%	-1.4%	+0.1%
			[3]		-6.4%		-6.5%	+129.3%	+28.3%	-4.5%	-1.6%
		30 μM	M1	-37.8%	-37.8%	+16.0%	+11.2%	+50.0%	-6.9%	-0.7%	-0.3%
			M2	-38.3%	-38.0%	-8.2%	-10.1%	-79.5%	+49.0%	-10.4%	+0.3%
			[3]		-38.0%		-18.7%	+475.6%	+53.3%	-21.0%	-6.3%
	1.0 Hz	10 μM	M1	-18.2%	-15.6%	+6.4%	+5.4%	+692.0%	+29.5%	-4.7%	-0.3%
			M2	-20.7%	-19.5%	-0.3%	-1.5%	+295.2%	+43.1%	-5.1%	+0.3%
			[3]		-17.9%	+7.2%	+1.2%	+135.8%	+36.1%	-5.4%	+0.7%
		30 μM	M1	-44.5%	-43.9%	+18.8%	+12.7%	+787.1%	+17.0%	-3.0%	-0.5%
			M2	-45.7%	-46.0%	-12.4%	-15.8%	+87.9%	+83.6%	-12.9%	+0.7%
			[3]		-45.6%	+11.0%	-4.1%	+430.2%	+63.3%	-18.6%	-2.9%
	3.0 Hz	10 μM	M1	-40.4%	-19.1%			+844.1%	+3.0%	-0.4%	+3.7%
			M2	-33.5%	-22.5%	-5.3%	-6.9%	+49.6%	+14.3%	-4.1%	+1.7%
			[3]		-22.1%	+10.7%	+11.2%	+90.1%	+4.6%	-8.2%	-3.2%
		30 μM	M1	-65.7%	-60.8%		+19.4%	+710.7%	-90.1%	+24.0%	+3.6%
			M2	-66.5%	-63.1%	-8.9%	-19.4%	+265.5%	+46.8%	-13.6%	+5.5%
			[3]		-62.7%	+31.3%	+15.0%	+100.8%	+52.5%	-36.1%	-10.4%
cAF	0.5 Hz	10 μM	M1	-7.1%	-7.2%	+11.6%	+11.9%	+52.3%	+3.2%	-1.7%	-0.1%
			M2	-7.2%	-7.3%	-8.7%	-9.3%	-29.3%	+6.3%	-1.7%	+0.0%
			[3]		-7.3%		+7.3%	+42.9%	+16.1%	-4.3%	-2.7%
		30 μM	M1	-23.4%	-23.2%	+18.0%	+16.6%	+75.7%	+17.5%	-5.9%	-0.1%
			M2	-37.5%	-24.2%	-17.4%	-20.8%	-45.6%	+20.5%	-6.5%	+0.0%
			[3]		-24.3%		+16.4%	+109.9%	-6.9%	-10.4%	-5.3%
	1.0 Hz	10 μM	M1	-11.9%	-13.2%	+12.4%	+12.7%	+47.5%	+7.2%	-2.9%	-0.1%
			M2	-10.3%	-10.9%	-9.5%	-10.5%	-27.7%	+10.0%	-2.5%	+0.1%
			[3]		-10.1%	+8.5%	+5.9%	+36.6%	+38.0%	-3.5%	-2.6%
		30 μM	M1	-31.2%	-31.0%	+18.9%	+17.3%	+67.1%	+25.7%	-8.2%	-0.1%
			M2	-29.8%	-30.9%	-19.5%	-23.1%	-46.6%	+26.7%	-7.9%	+0.1%
			[3]		-30.3%	+30.3%	+15.9%	+76.4%	+52.0%	-9.9%	-3.9%
	3.0 Hz	10 μM	M1	-16.0%	-15.3%	+11.6%	+10.5%	+56.5%	+13.2%	-4.2%	-0.3%
			M2	-19.1%	-18.5%	-5.4%	-7.4%	-7.1%	+16.8%	-4.6%	+0.4%
			[3]		-16.2%	+16.3%	+11.2%	+36.7%	+800.0%	-16.6%	-3.9%
		30 μM	M1	-43.4%	-44.2%	+15.6%	+10.6%	+107.8%	+41.0%	-12.1%	+0.4%
			M2	-44.0%	-45.3%	-15.0%	-21.4%	-11.9%	+42.8%	-11.8%	+1.2%
			[3]		-43.9%	+23.7%	+14.1%	+40.1%	+1070.0%	-16.6%	-14.3%

However, we did not observe the drug-induced increase of the divergence between ERP and APD_{90} (ERP prolongation accompanied by APD_{90} shortening) reported particularly for the *Control* substrate. Model M2 on the other hand covered the APD_{90} reduction as well as the increase of PLT_{20} whilst not replicating the ERP prolongation. The remaining AP markers were replicated sufficiently by both drug models.

4 Discussion

We showed how vernakalant prolongs the atrial refractory period by blocking the potassium currents I_{Kr}, I_{Kur}, and I_{to}, as well as the L-type calcium current I_{CaL} in a dose-dependent manner. Furthermore, I_{Na} is blocked frequency- and dose-dependently. This model based on literature data from the single channel level (M1) explains what can most probably be considered the major antiarrhythmic mode of action: ERP prolongation. Our results are in line with the in-vivo human data from Dorian et al. [4] describing a dose dependency but no pronounced frequency dependency of atrial ERP prolongation at frequencies between 1.6 and 3.3 Hz. Atrial ERP was prolonged by between 12 and 14% in [4] for the higher investigated intravenous dose of 4.6 mg/kg.

Our second drug model M2 was comprised of only I_{CaL} and I_{Na} block with values for I_{CaL} not being based on

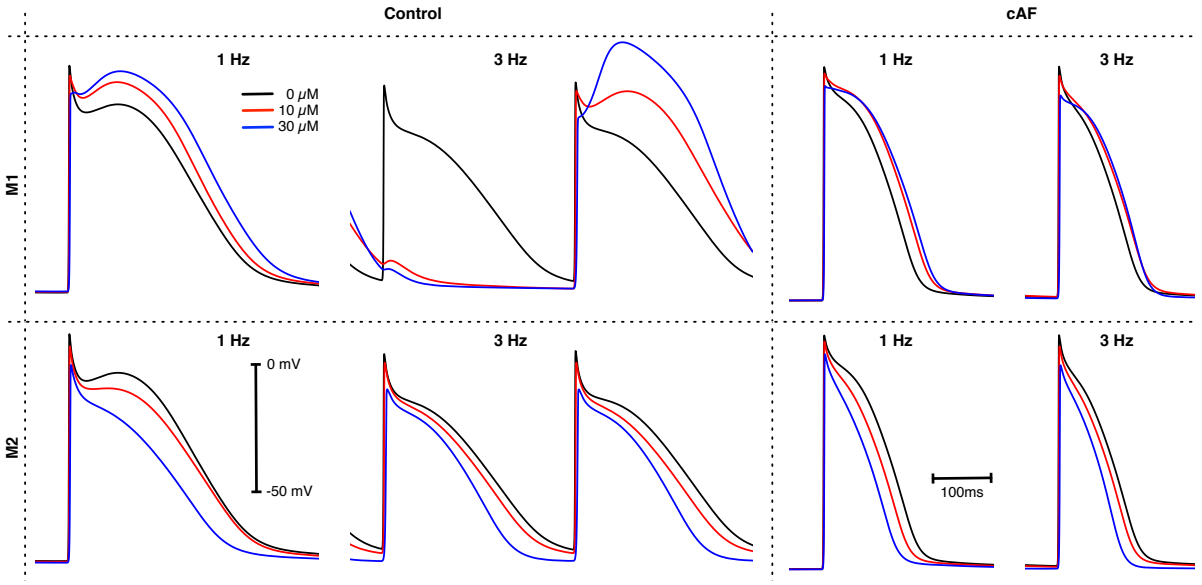

Figure 2: Vernakalant-induced change of the AP and its frequency dependence for the 2 drug models M1 and M2 in the Control and cAF substrates. AP curves are shown for the 5^{th} beat in the tissue strand. For 3 Hz in the Control substrate, the 6^{th} beat is shown as well because of 2:1 block using drug model M1.

subcellular experimental data but chosen to match experimentally observed AP morphology. This model provides a possible explanation of how APD_{90} and PLT_{20} are affected by vernakalant based on the delicate balance of inward and outward currents during the AP plateau and repolarization phase. PLT_{20} has to be considered with caution, though, as APD_{20} values differ significantly for some of the investigated combinations. Our findings are unlikely to be significantly affected by the choice of the atrial cell model as results using the model by Maleckar et al. [9] were very similar (data not shown).

While each of the models provides hypotheses for part of the experimentally observed characteristics, none of the setups is capable of reproducing and explaining the entirety of the observed effects. This fact reveals a missing piece of the puzzle in our understanding of vernakalant and throws up new questions. Future work might consider more complex drug models describing frequency-dependent block directly rather than using several Hill formulations. Another aspect, which might need to be covered in order to explain the experimentally observed increase in the difference between ERP and APD_{90} more comprehensively, is state-dependency.

In conclusion, our results foster the understanding of vernakalant's cellular mode of action and point out relevant gaps in our current knowledge. This study will thus hopefully fuel and direct future in-silico and experimental research on this aspiring antiarrhythmic agent.

Author's Statement

Conflict of interest: Authors state no conflict of interest. Material and Methods: Informed consent: Informed consent has been obtained from all individuals included in this study. Ethical approval: The research related to human use has been complied with all the relevant national regulations, institutional policies and in accordance the tenets of the Helsinki Declaration, and has been approved by the authors' institutional review board or equivalent committee.

References

[1] Camm, AJ et al.: 2012 focused update of the ESC guidelines for the management of atrial fibrillation. *Europace* 2012;14:1385–413.

[2] Fedida, D et al.: The mechanism of atrial antiarrhythmic action of RSD1235. *J Cardiovasc Elphysiol* 2005;16:1227–38.

[3] Wettwer, E et al.: The new antiarrhythmic drug vernakalant: ex vivo study of human atrial tissue from sinus rhythm and chronic atrial fibrillation. *Cardiovasc Res* 2013;98:145–54.

[4] Dorian, P et al.: The effect of vernakalant (RSD1235), an investigational antiarrhythmic agent, on atrial electrophysiology in humans. *J Cardiovasc Pharmacol* 2007;50:35–40.

[5] Courtemanche, M et al.: Ionic mechanisms underlying human atrial action potential properties: Insights from a mathematical model. *Am J Physiol* 1998;275:H301–21.

[6] Loewe, A et al.: Influence of chronic atrial fibrillation induced remodeling in a computational electrophysiological model. In

Biomed Eng, vol. 59. Walter de Gruyter, Berlin, Boston, 2014; S929–32.

[7] Seemann, G et al.: Framework for modular, flexible and efficient solving the cardiac bidomain equation using PETSc. *Math Ind* 2010;15:363–9.

[8] Loewe, A et al.: In-silico assessment of the dynamic effects of amiodarone and dronedarone on human atrial patho-electrophysiology. *Europace* 2014;16:iv30–8.

[9] Maleckar, MM et al.: K^+ current changes account for the rate dependence of the action potential in the atrial myocyte. *Am J Physiol Heart Circ Physiol* 2009;297:H1398–410.